2020

Driven Dipolariton Transistors in Y-shaped Channels

Patrick Serafin
CUNY New York City College of Technology

Tim Byrnes
New York University

German Kolmakov V
CUNY New York City College of Technology

Driven Dipolariton Transistors in Y-shaped Channels

Patrick Serafin,[1] Tim Byrnes,[2] and German V. Kolmakov[1]

[1]*Physics Department, New York City College of Technology, The City University of New York, Brooklyn, New York 11201, USA*
[2]*New York University Shanghai, 1555 Century Avenue, Pudong, Shanghai 200122, China*

(Dated: September 3, 2020)

Exciton-dipolaritons are investigated as a platform for realizing working elements of a polaritronic transistor. Exciton-dipolaritons are three-way superposition of cavity photons, direct and indirect excitons in a bilayer semiconducting system embedded in an optical microcavity. Using the forced diffusion equation for dipolaritons, we study the room-temperature dynamics of dipolaritons in a transition-metal dichalcogenide (TMD) heterogeneous bilayer. Specifically, we considered a $MoSe_2$-WS_2 heterostructure, where a Y-shaped channel guiding the dipolariton propagation is produced. We demonstrate that polaritronic signals can be redistributed in the channels by applying a driving voltage in an optimal direction. Our findings open a route towards the design of an efficient room-temperature dipolariton-based optical transistor.

I. INTRODUCTION

Semiconductor technology has allowed for the innovation of devices such as light emitting diodes[1,2], lasers[3,4], and polarization rectifiers[5]. The emerging field of polaritronics has opened the route towards the use of polaritons in many innovative structures[6]. Research into exciton-polariton dynamics has allowed for the observance of their rich physical phenomena, such as Bose-Einstein condensate superfluidity[7], quantum vortices[8], lasing capabilities[9], and novel many-body physics[10–12]. In addition, exciton-polariton transport has been investigated in a variety of novel materials[13–15] and has sparked interest in the study of their manipulation and trapping within semiconductor microcavities[16]. The potential for use of exciton-polaritons in a wide array of applications such as quantum information[17], polariton lasers[18], tunneling diodes[19], and optical transistors[20] has led to study and review of their properties and phenomenology[21]. Atomtronics, the atomic counterpart of polaritronics, has led to various quantum technology applications[22] such as atomtronic batteries[23] and circuits[24]. In this report we narrow our attention to the study of polaritronics, specifically, we investigate exciton-polariton dynamics.

The emergence of transition metal dichalcogenides (TMDs) provide unique opportunities to realize many proposed applications[25,26] of exciton and polariton physics to room-temperature scales. Unique properties of TMDs include large exciton binding energy ~ 1 eV[27] and large vacuum Rabi splitting energy ~ 100 meV[28]. Tungsten based-TMDs heterostructures provide near degenerate interlayer and intralayer excitionic states, which enables one to dynamically tune these states via the application of an electric field normal to the layers or the gate voltage[29]. In particular, it has been found that TMD heterostructures possess band alignments that allow for spatial separation between the electrons and holes in the TMD layers upon lasing[29].

In this paper, we study propagation of polaritons in $MoSe_2$-WS_2 heterogeneous bilayer structures embedded in an optical microcavity. Dipolaritons are quasiparticles with a three-way superposition of cavity photons, intralayer (direct) and interlayer (indirect) excitons as seen in Fig.1[30,31]. Additionally, the band diagram for $MoSe_2$-WS_2 provides for a clear visual representation of the formation of dipolaritons present in our system[32]. The advantage of dipolaritons lie in the possibility to directly apply an electric force due to the driving electric voltage applied to one of the layers[33]. The latter makes dipolaritons a promising candidates for polaritronic, optoelectronic, and photonic applications[31]. In our approach, the heterostructure possesses a Y-shaped channel guiding the dipolariton propagation. Y-shaped channels were recently proposed to guide exciton polariton propagation in gallium-arsenide (GaAs) based microcavities at liquid helium temperatures[34]. In the present work, we numerically investigate an electrically controlled optical switch based on dipolaritons in $MoSe_2$-WS_2 heterostructures in an optical cavity, which are able to operate at room temperatures[35,36]. In particular we show the optimal system parameters that enable the efficient re-routing of dipolaritons in the Y-shaped channel of the TMD heterostructure.

II. DIPOLARITON DIFFUSION IN A TMD HETEROSTRUCTURE EMBEDDED IN AN OPTICAL CAVITY

We consider the motion of dipolaritons under the action of an external electric field generated by a voltage applied to the system acting on the charges located in the $MoSe_2$ layer in the $MoSe_2$-WS_2 heterostructure as illustrated in Fig. 2. The direct excitons are created by laser radiation in the excitation spot of characteristic size $\sim 10 - 20$ μm at the stem of the channel, as described below. The interaction of the polaritons with uncoupled excitons can significantly modify the character of the polariton motion if they are located in the same spatial domain[37]. However, from the simulations below it follows that in our case the dipolaritons travel in the

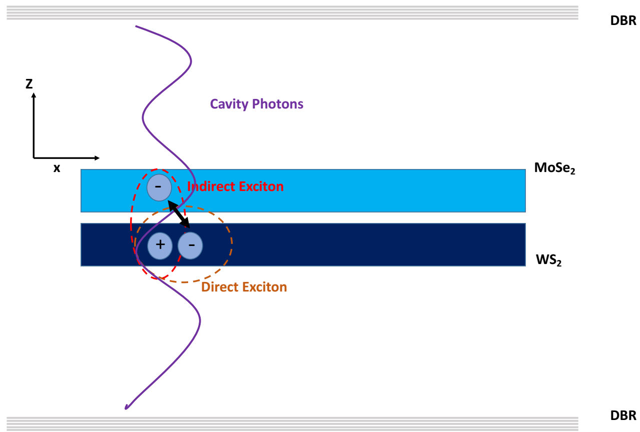

FIG. 1. Schematic showing the physical process for generating dipolaritons. Spatially separated electrons and electron holes of type II-band alignments between the monolayers of the TMD are photoexcited generating indirect excitons and direct excitons. Coupling of direct excitons with the cavity photons generate a three-way superposition of direct exciton, indirect excitons, and cavity photons. The application of an external voltage provides for a driving force on the dipolaritons which are guided by the Y-shaped channel. The thick arrow between the indirect exciton and the direct exciton indicates the ability of the electron to tunnel between layers with probability given by the Hopfield coeffcient $|Y|^2$, as described in (8). The dotted lines around the direct exciton and indirect exciton represent bounding by the Coulomb charge.

channel over the distances $\sim 100-500$ μm under the action of the electric driving force generated by the application of an external voltage as seen in Fig. 2. This distance is much larger than the size of the direct and indirect excitons. Thus, the dipolaritons propagate in the area where the uncoupled exciton density is negligible and the effect of the exciton-dipolariton interaction can be disregarded. Therefore, in the simulations we omit the exciton-dipolariton coupling in the channel and only consider the dipolariton dynamics.

In this work we follow the approach of modeling the dynamics of the dipolariton gas using the semi-classical stochastic differential equation for the polariton wave packet[38]:

$$\dot{\mathbf{r}}(t) = \eta_{\rm dip}\mathbf{F}(\mathbf{r}(t), t))dt + \sqrt{2D}d\mathbf{W}(t), \quad (1)$$

where $\mathbf{F}(\mathbf{r}$,t) is the external force acting on the dipolaritons, $\eta_{\rm dip}$ is the dipolariton mobility, D is the diffusivity, and $d\mathbf{W}(t)$ the differential of a Weiner process[38]. The force acting on polaritons is set to $\mathbf{F} = -\nabla U_{\rm eff}(r)$. The laser light spot polariton source is modeled by the addition of particles for each time step δt with a Gaussian probability distribution. The lower dipolariton mass depends on the effective cavity photon mass $m_{\rm ph} = \sqrt{\epsilon}\pi\hbar/cL_C$ and the exciton mass $m_{\rm ex}$=$m_{\rm e}$+$m_{\rm h}$ as follows[31].

$$\frac{1}{m} = \frac{|C|^2}{m_{\rm ph}} + \frac{|X|^2 + |Y|^2}{m_{\rm ex}}. \quad (2)$$

Here, ϵ is the dielectric constant of the host material, c is the speed of light, L_C is the cavity length, $m_{\rm e(h)}$ is the electron (hole) mass, where we take $m_{\rm ex}$=0.7m with $m_{\rm ex}$ as the free electron mass, and $m_{\rm ph}$ is the photon mass. The Hopfield coefficients C, X, and Y for the photon, direct and indirect excitons in the dipolariton wave function depend on dipolariton momentum and on the detuning in the system. In the case of zero detuning for both the photons and indirect excitons and low momentum, the typical values are $|X|^2 = 1/2$, $|C|^2 = |Y|^2 = 1/4$[31]. The dipolariton momentum relaxation time $\tau_{\rm dip}$ depends on the photon $\tau_{\rm ph}$, direct exciton $\tau_{\rm DX}$, and indirect exciton $\tau_{\rm IX}$ lifetimes as

$$\frac{1}{\tau_{\rm \ dip}} = \frac{|C|^2}{\tau_{\rm ph}} + \frac{|X|^2}{\tau_{\rm DX}} + \frac{|Y|^2}{\tau_{\rm IX}}. \quad (3)$$

In the simulations, the momentum relaxation times for the direct and indirect excitons and cavity photons were taken as $\tau_{\rm DX}$ = 4 ps, $\tau_{\rm IX}$ = 80 ps and $\tau_{\rm ph}$ = 100 ps, respectively[29,39]. The dipolariton diffusivity is calculated as[38]

$$D = \frac{m_{\rm ex}}{m}|X^{-4}|D_{\rm ex}, \quad (4)$$

where $D_{\rm ex}$ is the exciton diffusion coefficient, with $X = 1/\sqrt{2}$ as we consider zero detuning between the excitonic and photonic resonances. The dipolariton mobility is calculated as[38]

$$\eta_{\rm dip} = \frac{\tau_{\rm dip}}{m}, \quad (5)$$

for $\tau_{\rm dip}$ where $\tau_{\rm dip}$ is the momentum relaxation time of the dipolaritons.

The effective potential $U_{\rm eff}(\boldsymbol{r})$ captures the effects of patterning of the microcavity and of the coordinate dependence of the electrochemical potential of the dipolaritons,

$$U_{\rm eff}(\boldsymbol{r}) = U_{\rm conf}(\boldsymbol{r}) + \mu_{\rm e-chem}(\boldsymbol{r}). \quad (6)$$

The confining potential due to patterning, $U_{\rm conf}(\boldsymbol{r})$ is shown in Fig. 2. In the case where the drive voltage is applied across the electron-carrying quantum well, the electrochemical potential in the system is

$$\mu_{\rm e-chem}(\boldsymbol{r}) = \mu_0 + e|Y|^2\phi(\boldsymbol{r}), \quad (7)$$

where μ_0 is the chemical potential of dipolaritons. In what follows we consider the case where no voltage is applied across the layer, which carries the holes. The factor $|Y|^2$ in Eq. (7) is the probability for the electron to be located in the electron-carrying TMD layer. The effective drive force acting on the dipolaritons is

$$\boldsymbol{F} = -\nabla\mu(\boldsymbol{r}) = e|Y|^2\boldsymbol{E}, \quad (8)$$

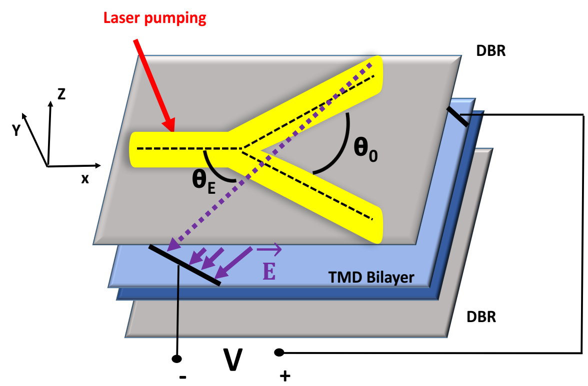

FIG. 2. Schematic of a TMD heterogenous bilayer embedded inside an optical microcavity with a Y-shaped channel guiding the dipolaritons. The opening angle of the channel is $\theta_0 = 30$ and the direction of the field $\boldsymbol{E}$ generated by an external voltage applied to the bilayer is defined by an angle θ_E between the field vector and the direction of the stem of the Y-shaped channel. The direction of the electric driving force applied to the dipolaritons is opposite to the direction of the electric field. Distributed Bragg Reflectors (DBR) are placed between the TMD bilayer and laser pumping is applied to generate dipolaritons, at the beginning of the stem of the channel at which point they propagate along the x-axis towards the junction under the action of the electric field $\boldsymbol{E}$.

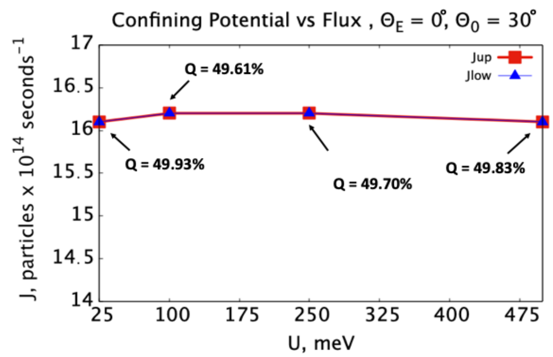

FIG. 3. Confining potential U versus flux J for the case of the opening angle of the channel, θ_0= 30° and the electric field angle, $\theta_E = 0°$. The flux through the upper branch of the Y-shaped channel is labeled as "$J_{\rm up}$" and the flux through the lower branch of the Y-shaped channel is labeled as "$J_{\rm low}$". The performance Q is indicated by the arrows pointing to the overlapping flux points.

where the electric field in the system is $\boldsymbol{E} = -\nabla\phi(\boldsymbol{r})$. In this paper, we consider the simplest case where the electric field $\boldsymbol{E}$ is uniform. The source of the dipolaritons $P(\boldsymbol{r})$ was taken in the form of a Gaussian function centered at the base of the stem (see Fig. 2) with the full width at half maximum (FWHM) of 16.7 μm

Furthermore, we consider zero detunings where the cavity photons and the excitons are in resonance at $\boldsymbol{k} = 0$.

To characterize the flow of the dipolariton condensate in the channel, we calculated the total dipolariton flux through the upper (lower) branches of the Y-channel junction

$$J = \int da j_{||}, \tag{9}$$

where the integration is performed along the cross-section of the branches, da is the area being integrated over and $j_{||} = \boldsymbol{j} \cdot \boldsymbol{\nu}$ is the component of the dipolariton flux along the channel. The angles θ_0 and θ_E are only included in our numerical modeling of the Y-channel structure that the condensate flows in and does not find direct applicability in Eq.(9).

The flux in our simulation is found by simple averaging of particles. We adopt the notation of $\Delta J dt = \pm 1$ and

TABLE I. Simulation parameters for a cavity with embedded $MoSe_2$-WS_2 bilayer

Quantity name	Value	Variable
Exciton mass	$m_{\rm ex}$	$0.70 m_0$
Photon mass	$m_{\rm ph}$	$1.1234 \times 10^{-5} m_0$
Dipolariton mass	m	$2.4 \times 10^{-5} m_0$
Dipolariton lifetime	$\tau_{\rm dip}$	15.64×10^{-12} s
Indirect exciton lifetime	$\tau_{\rm IX}$	80×10^{-12} s
Direct exciton lifetime	$\tau_{\rm DX}$	4.0×10^{-12} s
Cavity Photon lifetime	$\tau_{\rm ph}$	100×10^{-12} s
Exciton diffusion coefficient	$D_{\rm ex}$	14 $\rm cm^2/s$
Dimensionless dipolariton diffusion coefficient	$D \times dt/dx^2$	271.7
Dimensionless dipolariton mobility	$\eta_{\rm dip} \times eVdt/dx$	0.0015
Dielectric constant	ϵ	4
Exciton Energy	$E_{\rm ex}$	1.58eV
Confining potential	U	$25 - 500 meV$
Numerical unit of length	dx	0.15 μm
Numerical time step	dt	9.63 fs

define $J_{\rm up}dt = +1$ and $J_{\rm low}dt = -1$, where ± 1 is taken in numerical units, with 1 numerical unit $= 9.6 \times 10^{15}$ dipolariton particles per second. When the system comes to a steady state, particles found at $x > x_{\rm j}$, $y > y_{\rm j}$ are counted as $J_{\rm up}$, where $x_{\rm j} = 450\mu$m, $y_{\rm j} = 225\mu$m. The counting locations for $x_{\rm j}$ and $y_{\rm j}$ were selected as to ensure the particles would be at a location past the junction of the Y-channel to accurately record them as being either through the upper or lower branch of the Y-channel, rather than at some location along the stem of Y-channel. Particles found at $x < x_j$, $y > y_j$, are counted as $J_{\rm up}$. Particles found at $x > x_{\rm j}$, $y < y_{\rm j}$ are counted as $J_{\rm low}$ and

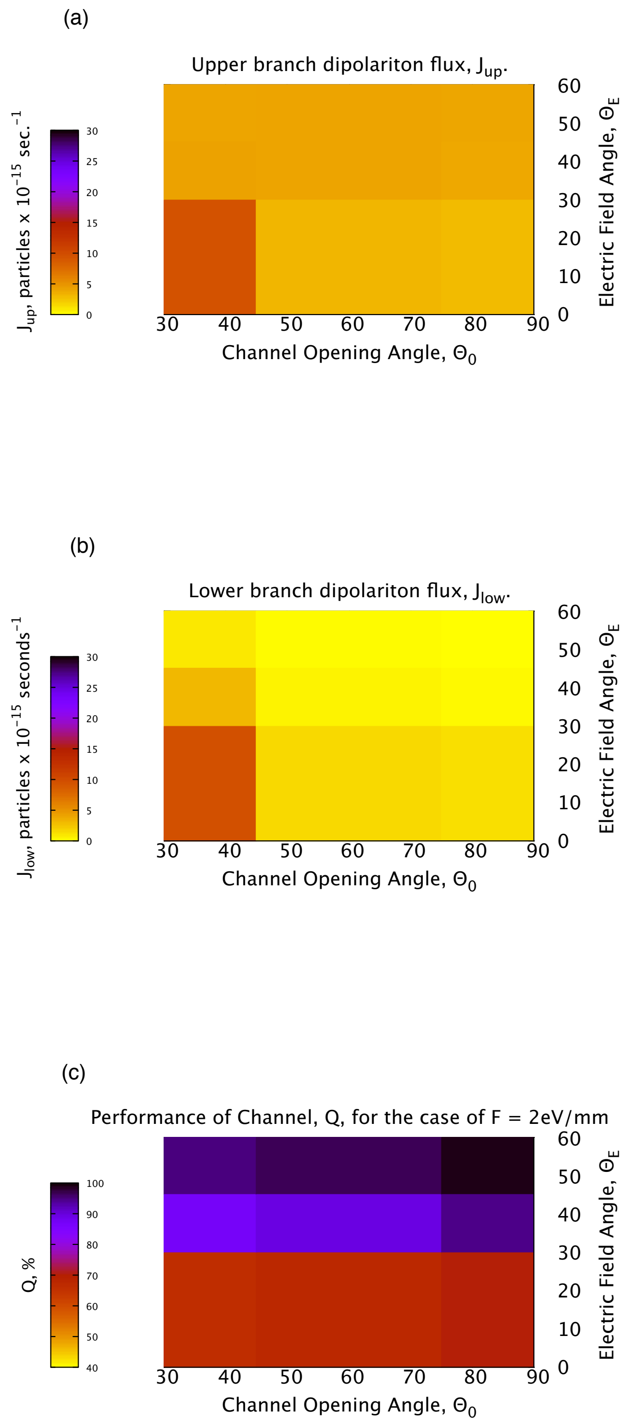

FIG. 4. (a) the upper dipolariton flux, (b) lower dipolariton flux in the Y-channel as functions of the channel opening angle and electric field angle with the electric driving force F set to 2eV/mm. (c) The performance of the channel as a function of the opening angle and electric field angle with the driving force set to $F = 2$eV/mm. The performance in (c) as defined in (11) is calculated using the upper and lower dipolariton flux plots.

particles found at $x < x_j$, $y < y_j$ are counted as J_{low}. More compactly, this counting scheme can be expressed as

$$\Delta J dt = \mathrm{sgn}(x - x_j)\mathrm{sgn}(y - y_j). \tag{10}$$

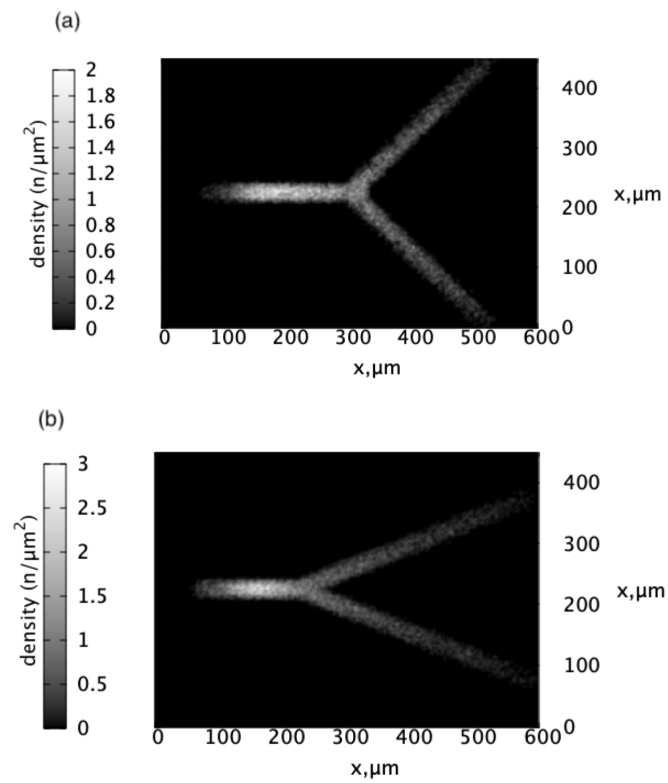

FIG. 5. Steady-state dipolariton condensate flow in at the Y-shaped channel in a $MoSe_2$-WS_2 based microcavity for (a) an opening angle of $\theta_0 = 90^o$, driving force $F = 1.0$eV/mm, electric field angle $\theta_0 = 0^o$ and (b) an opening angle of $\theta_0 = 45^o$, driving force $F = 0.5$eV/mm, electric field angle $\theta_0 = 90^o$. The gradient bars on the left of the plots labeled with units $n/\mu m^2$, the number of particles per micron-squared, display the dipolariton condensate density.

To characterize the redistribution of the dipolariton flux in the channel in response to F, we calculated the fraction of dipolaritons propagating through the upper branches, or what we define as the performance, as

$$Q = \frac{J_{up}}{J_{up} + J_{low}} \times 100\%. \tag{11}$$

We define Q in such a manner in order to find the percentage of dipolariton flux going through the upper branch of the channel relative to the overall dipolariton flux in the Y-shaped channel. This enables us to quantify to what extent we can re-route the total dipolariton flux in the channel through the upper branch of the Y-shaped channel.

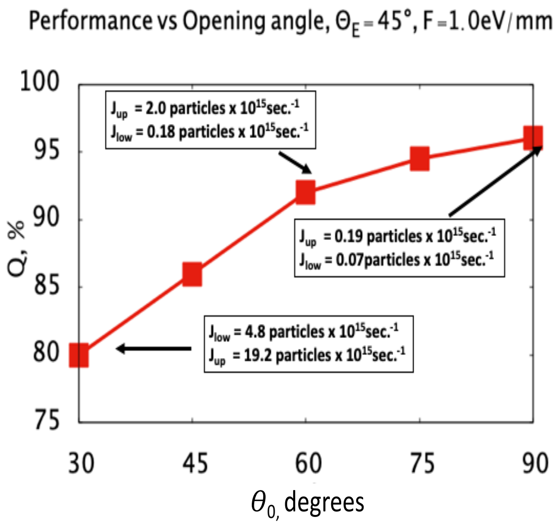

FIG. 6. Performance Q versus opening angle, θ_0, for the case $\theta_E = 45^o$ and $F = 1.0$eV/mm. Arrows point to the fluxes, $J_{\rm up}$ and $J_{\rm low}$, for corresponding Q values.

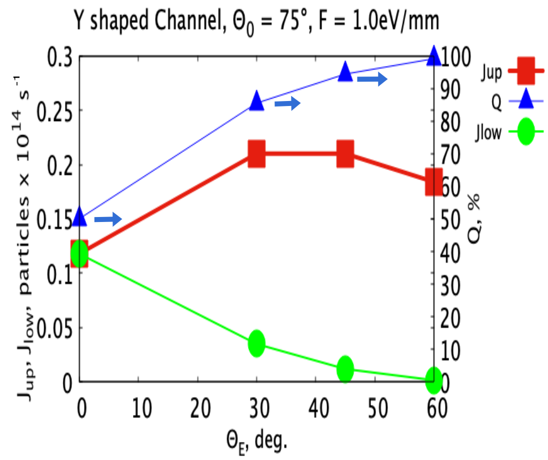

FIG. 7. Dipolariton flux through the upper and lower branches of the Y-shaped channel, $J_{\rm up}$ and $J_{\rm low}$, and the Q factor as functions of the direction of the in-plane electric field, θ_E, for the case $\theta_0 = 75^o$ and F = 1.0eV/mm. The blue arrows point to the y_2 axis indicating flux for the value.

In the simulations, we set the maximum depth of confining potential $U_{\rm conf}(\boldsymbol{r})$ equal to 250 meV. To study the effect of the confining potential depth on the dipolariton flow we varied its value from 25 meV to 500 meV. We found statistically insignificant differences in performance Q, as defined in Eq.(11), and dipolariton fluxes, J as defined in Eq.(10) for this range of confining potential as shown in Fig 3. Thus, we can claim that our results very weakly depend on the confining potential. The simulation parameters are shown in Table 1.

III. OPTIMIZING THE PERFORMANCE OF THE Y-CHANNEL TO EFFECTIVELY REROUTE DIPOLARITONS

In order to determine the optimal condition for directing dipolaritons in the Y-shaped channel, we varied θ_0, the opening angle of the channel, from $\theta_0 = 30^o$ to $\theta_0 = 90^o$. The cases of $\theta_0 < 30^o$ were not investigated as the $\theta_0 = 30^o$ was chosen to be the lowest opening angle that still maintains our channel classification as one possessing a Y-shaped channel. The plots in Fig. 5 illustrate the condensate density for the Y-shaped channel and serve as a visual representation of the condensate when varying system parameters in our optical microcavity. The behavior of the channel can be summarized in Fig.4(a)-(c) where we can observe the dipolariton fluxes and the channel performance as functions of channel opening angle and electric field angle. We can see in Fig. 4(c) that the performance Q is optimized when the electric field angle and opening angle are maximized. Further, we can see that Q has values greater than 90% when the electric field angle is at 60^o irrespective of the field angle when the driving force is greater than 2eV/mm. It is interesting to note, however, that both upper and lower dipolariton flux is maximized at channel opening angles and electric field angles of 60^o . This can be understood by noting that an increased opening angle requires the dipolaritons to travel farther from the initial excitation spot in order to pass through the branches of the channel with an increased opening angle. In what follows we will investigate and cite results for particular case studied; that is, cases where the electric field angle $\theta_{\rm E}$, the channel opening angle θ_0, and electric driving force F, are varied. In particular, we numerically calculated the performance Q as a function of θ_0 for the case of $\theta_E = 45^o$ and $F = 1.0$eV/mm. As illustrated in Fig. 6, we can see that Q is maximized for the case of $\theta_0 = 90^o$ where Q reaches a value of $\approx 96\%$. Furthermore, we see that the lowest value of the opening angle, $\theta_0 = 30^o$, provides for a minima for this case where the performance reaches $Q \approx 80\%$. Thus, we can claim that Q, the performance, monotonically increases with the opening angle of the channel for the range we investigated of $\theta_0 = 30^o$ to 90^o where we can observe that performance can be improved by up to 16%. It is noteworthy, however, to observe that the flux of particles through the upper and lower branch,

$J_{\rm up}$ and $J_{\rm low}$, decreases with increase of θ_0 as seen in Fig. 6. We can see that the flux of particle for the case of $\theta_0 = 30^{\rm o}$ is substantially higher than the flux of particles for the other opening angles. In particular, from Fig. 6 we can see that for $\theta_0 = 30^{\rm o}$ $J_{\rm up}$ and $J_{\rm low}$ reach values of 19.2 $\times$ 10^{15} $\rm s^{-1}$ particles and 4.8 $\times$ 10^{15} $\rm s^{-1}$particles, respectively, compared to $\theta_0 = 90^{\rm o}$ where $J_{\rm up}$ and $J_{\rm low}$ reach values of $0.19 \times 10^{15}\rm s^{-1}$particles and $0.07 \times 10^{15}\rm s^{-1}$ particles, respectively. Thus, an increase in the opening angle of the channel lowers the flux of dipolaritons in the channel while increasing the performance.

In order to test efficacy of increasing θ_0 on Q for different parameters, we numerically computed Q as a function of θ_0 for the case of $\theta_E = 0^{\rm o}$ and $F = 1.0$eV/mm. It was found that for a value of $\theta_{\rm E} = 0^{\rm o}$, the increase in Q, is minimal, although still monotonically increasing with θ_E. We can observe an increase in performance of $\Delta Q \approx$1.3% as $\theta_0 = 30^{\rm o}$ is increased to $\theta_0 = 90^{\rm o}$. Thus, we can claim that an increase in performance from a wider opening angle of the channel must be accompanied by a non-zero electric field angle in order to appreciate Q significantly.

In order to find an optimum in Q as a function of the electric field angle, $\theta_{\rm E}$, we numerically calculated the performance Q of the Y-shaped channel as a function of the electric field angle $\theta_{\rm E}$. Fig. 7 shows the fluxes $J_{\rm up}$ and $J_{\rm low}$ and the performance Q as function of the electric field angle $\theta_{\rm E}$. We can see that both Q and $J_{\rm up}$ are a monotonically increasing functions with θ_E whilst $J_{\rm low}$ is a montonically decreasing function with $\theta_{\rm E}$. In particular, we can claim an increase in performance of ≈50% as we increase the angle of the electric field from $\theta_{\rm E} = 0^\circ$ to $\theta_{\rm E} = 60^\circ$. Fig. 7 shows that the flux through the upper branch, $J_{\rm up}$ is increased by $\approx 0.63 \times 10^{15}$ $\rm s^{-1}$ particles as we increase the angle of the electric field from $\theta_{\rm E} = 0^\circ$ to $\theta_E = 60^\circ$. Inspection of Fig. 7 reveals that the most performance per increase in electric field angle occurs in the range of $\theta_{\rm E} = 0^\circ$ to $\theta_{\rm E} = 30^\circ$ as Q is appreciated by ≈31%. The increase of θ_E from 30° to 45° increases performance by ≈ 9% and the increase of $\theta_{\rm E}$ from 45° to 60° increases performance by ≈5%. Thus, for practical matters, the most substantial increase in performance occurs in the range $\theta_{\rm E} = 0^\circ$ to $\theta_{\rm E} = 30^\circ$ with an optimum in performance for $\theta_{\rm E} = 60^\circ$. Thus, we can claim that an increase of the electric field angle appreciates the performance to a higher extent than increasing the opening angle and increases the flux of dipolaritons in the channel.

In order to find an optimum in Q as a function of the driving force F on dipolaritons, we numerically calculated the performance of the Y-shaped channel as a function of the driving force on dipolaritons. In Fig. 8 we can can see the performance as a function of the driving force. In particular, we see that Q, $J_{\rm up}$ and $J_{\rm low}$ are monotonically increasing with F. In particular, we can observe an improvement of performance of ≈ 8.5% for an increase in driving force from 500meV/mm to 2000meV/mm. We can also report an increase in the flux of particles, $J_{\rm up}$ and $J_{\rm low}$, of ≈ 3.3× 10^{15} $\rm s^{-1}$ particles and 0.7× 10^{15} $\rm s^{-1}$ particles, respectively. This dependence has also been observed for other opening angles and electric field angles. Thus, we can claim that an increase in the driving force on the channel can increase both the flux of dipolaritons and the performance of the channel.

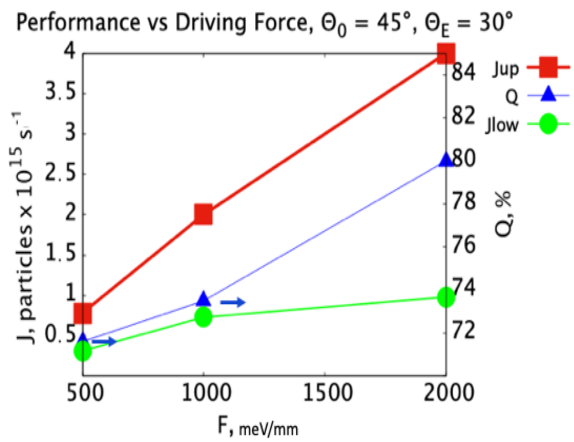

FIG. 8. Dipolariton flux through the upper and lower branches of the Y-shaped channel, J_{up} and J_{low}, and the Q factor as functions of the direction of the driving force, F, for the case $\theta_0 = 45^\circ$ and $\theta_E = 30^\circ$. The blue arrows point to the y_2 axis indicating flux for the value

Based on our variation of channel parameters, we were able to find optimal conditions for performance. We report these optimal parameters in Fig. 9 where we found our optimum conditions as $\theta_E = 60^{\rm o}$, $\theta_0 = 90^{\rm o}$, and $F = 2.0$eV/mm. We can report that Q reaches a maxima of ≈ 100% when $\theta_E = 60^{\rm o}$, whilst the minima of this case is in the usual vicinity of ≈ 50%. Furthermore, it is noteworthy that the performance reaches ≈ 92% for the electric field angle of $\theta_E = 30^{\rm o}$, which is larger than the cases in Fig. 9, where θ_E is held fixed at $\theta_E = 30^{\rm o}$.

IV. CONCLUSIONS

By considering dipolariton propagation in a Y-shaped TMD channel embedded in an planar optical microcavity, we demonstrated that the dipolariton flow can be efficiently re-routed by applying the electric field driving force ∼ 2 eV/mm at angle $\theta_E = 60^\circ$ and an opening angle of $\theta_0 = 90^\circ$. As TMDs have been shown to function at room temperature[35], the dipolariton switch we have investigated will likewise be able to operate at room temperature. There is an optimum in the angle of the electric field direction, θ_E, for the Y-shaped channel for which the value of Q is maximized. Thus, when the electric force acting on dipolaritons is 2eV/mm with θ_E

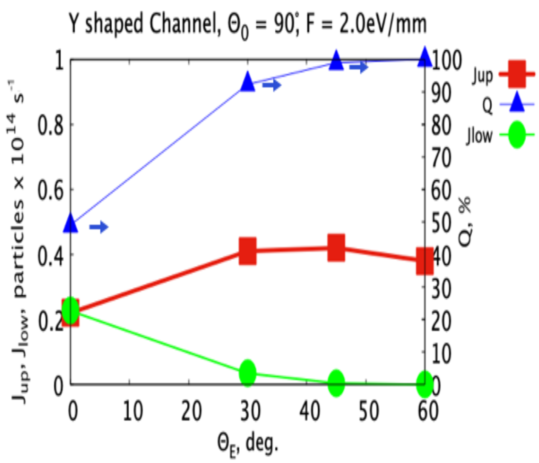

FIG. 9. Dipolariton flux through the upper and lower branches of the Y-shaped channel, J_{up} and J_{low}, and the Q factor as functions of the electric field angle, θ_E, for the case $\theta_0 = 90°$ and F = 2.0eV/mm . The blue arrows point to the y_2 axis indicating flux for the value

= 60°, about 100% of dipolaritons can be switched in the desired direction in the channel for all opening angles of the channel.

The value of Q monotonically increases with an increase of θ_E for most cases investigated in the Y-channel; in particular, this monotonicity is only broken for θ_0 = 60° where the conditions in the channel are F = 2eV/mm, θ_E = 60°, F = 2 eV/mm, θ_E = 45°, and F = 1 eV/mm, θ_E = 60°. This can attributed to the stochastic and random nature of the system in question. Outside the optimal condition parameter range, the efficiency Q and dipolaritons cannot be efficiently re-routed in the channel. Our consideration opens a route to the design of efficient room-temperature optoelectronic applications, including optical routers and switches, based on dipolaritons in TMD microcavities.

V. ACKNOWLEDGMENTS

This work was supported in part by the Department of Defense under the grant No. W911NF1810433. The authors are grateful to The Center for Theoretical Physics New York City College of Technology of The City University of New York for providing computational resources. The authors are also grateful to R. Ya. Kezerashvili and O. L. Berman for fruitful discussions.

[1] S. I. Tsintzos, N. T. Pelekanos, G. Konstantinidis, Z. Hatzopoulos, and P. G. Savvidis. A GaAs polariton light-emitting diode operating near room temperature. *Nature*, 453(7193):372–375, May 2008.

[2] Rahul Jayaprakash, Kyriacos Georgiou, Harriet Coulthard, Alexis Askitopoulos, Sai K. Rajendran, David M. Coles, Andrew J. Musser, Jenny Clark, Ifor D. W. Samuel, Graham A. Turnbull, Pavlos G. Lagoudakis, and David G. Lidzey. A hybrid organicinorganic polariton LED. *Light: Science & Applications*, 8(1):1–11, September 2019.

[3] Daniele Bajoni, Pascale Senellart, Esther Wertz, Isabelle Sagnes, Audrey Miard, Aristide Lemaître, and Jacqueline Bloch. Polariton laser using single micropillar GaAs−GaAlAs semiconductor cavities. *Phys. Rev. Lett.*, 100:047401, Jan 2008.

[4] A. A. Khalifa, A. P. D. Love, D. N. Krizhanovskii, M. S. Skolnick, and J. S. Roberts. Electroluminescence emission from polariton states in GaAs-based semiconductor microcavities. *Applied Physics Letters*, 92(6):061107, February 2008.

[5] Evgeny S. Sedov, Yuri G. Rubo, and Alexey V. Kavokin. Polariton polarization rectifier. *Light: Science & Applications*, 8(1):1–10, August 2019.

[6] Daniele Sanvitto and Stphane Kna-Cohen. The road towards polaritonic devices. *Nature Materials*, 15(10):1061–1073, October 2016.

[7] Alberto Amo, Jrme Lefrre, Simon Pigeon, Claire Adrados, Cristiano Ciuti, Iacopo Carusotto, Romuald Houdr, Elisabeth Giacobino, and Alberto Bramati. Superfluidity of polaritons in semiconductor microcavities. *Nature Physics*, 5(11):805–810, November 2009.

[8] K. G. Lagoudakis, M. Wouters, M. Richard, A. Baas, I. Carusotto, R. Andr, Le Si Dang, and B. Deveaud-Pldran. Quantized vortices in an excitonpolariton condensate. *Nature Physics*, 4(9):706–710, September 2008.

[9] S. Christopoulos, G. Baldassarri Höger von Högersthal, A. J. D. Grundy, P. G. Lagoudakis, A. V. Kavokin, J. J. Baumberg, G. Christmann, R. Butté, E. Feltin, J.-F. Carlin, and N. Grandjean. Room-temperature polariton lasing in semiconductor microcavities. *Phys. Rev. Lett.*, 98:126405, Mar 2007.

[10] Tim Byrnes, Tomoyuki Horikiri, Natsuko Ishida, and Yoshihisa Yamamoto. BCS Wave-Function Approach to the BEC-BCS Crossover of Exciton-Polariton Condensates. *Physical Review Letters*, 105(18):186402, October 2010.

[11] Natsuko Ishida, Tim Byrnes, Tomoyuki Horikiri, Franco Nori, and Yoshihisa Yamamoto. Photoluminescence of high-density exciton-polariton condensates. *Physical Review B*, 90(24):241304, December 2014.

[12] Tim Byrnes, Tomoyuki Horikiri, Natsuko Ishida, and Yoshihisa Yamamoto. Bcs wave-function approach to the bec-bcs crossover of exciton-polariton condensates. *Physical Review Letters*, 105(18):186402, October 2010.

[13] Naoyuki Masumoto, Na Young Kim, Tim Byrnes, Kenichiro Kusudo, Andreas Lffler, Sven Hfling, Alfred Forchel, and Yoshihisa Yamamoto. Exciton–polariton condensates with flat bands in a two-dimensional kagome lattice. *New Journal of Physics*, 14(6):065002, jun 2012.

[14] Weiliang Ma, Pablo Alonso-Gonzlez, Shaojuan Li, Alexey Y. Nikitin, Jian Yuan, Javier Martn-Snchez, Javier Taboada-Gutirrez, Iban Amenabar, Peining Li, Sal Vlez, Christopher Tollan, Zhigao Dai, Yupeng Zhang, Sharath Sriram, Kourosh Kalantar-Zadeh, Shuit-Tong Lee, Rainer Hillenbrand, and Qiaoliang Bao. In-plane anisotropic and ultra-low-loss polaritons in a natural van der Waals crystal. *Nature*, 562(7728):557–562, October 2018.

[15] Vincenzo Ardizzone, Luisa De Marco, Milena De Giorgi, Lorenzo Dominici, Dario Ballarini, and Daniele Sanvitto. Emerging 2D materials for room-temperature polaritonics. *Nanophotonics*, 8(9):1547–1558, July 2019.

[16] Na Young Kim, Chih-Wei Lai, Shoko Utsunomiya, Georgios Roumpos, Michael Fraser, Hui Deng, Tim Byrnes, Patrik Recher, Norio Kumada, Toshimasa Fujisawa, and Yoshihisa Yamamoto. GaAs microcavity exciton-polaritons in a trap. *physica status solidi (b)*, 245(6):1076–1080, 2008.

[17] Frederick Ira Moxley, Jonathan P. Dowling, Weizhong Dai, and Tim Byrnes. Sagnac interferometry with coherent vortex superposition states in exciton-polariton condensates. *Phys. Rev. A*, 93:053603, May 2016.

[18] Michael D. Fraser, Sven Hfling, and Yoshihisa Yamamoto. Physics and applications of excitonpolariton lasers. *Nature Materials*, 15(10):1049–1052, October 2016.

[19] H. S. Nguyen, D. Vishnevsky, C. Sturm, D. Tanese, D. Solnyshkov, E. Galopin, A. Lemaître, I. Sagnes, A. Amo, G. Malpuech, and J. Bloch. Realization of a double-barrier resonant tunneling diode for cavity polaritons. *Phys. Rev. Lett.*, 110:236601, Jun 2013.

[20] Anton V. Zasedatelev, Anton V. Baranikov, Darius Urbonas, Fabio Scafirimuto, Ullrich Scherf, Thilo Stferle, Rainer F. Mahrt, and Pavlos G. Lagoudakis. A room-temperature organic polariton transistor. *Nature Photonics*, 13(6):378–383, June 2019.

[21] Tim Byrnes, Na Young Kim, and Yoshihisa Yamamoto. Excitonpolariton condensates. *Nature Physics*, 10(11):803–813, November 2014.

[22] Luigi Amico, Gerhard Birkl, Malcolm Boshier, and Leong-Chuan Kwek. Focus on atomtronics-enabled quantum technologies. *New Journal of Physics*, 19:020201, 2017.

[23] Seth C Caliga, Cameron J E Straatsma, and Dana Z Anderson. Experimental demonstration of an atomtronic battery. *New Journal of Physics*, 19(1):013036, jan 2017.

[24] R. A. Pepino, J. Cooper, D. Z. Anderson, and M. J. Holland. Atomtronic circuits of diodes and transistors, 2007.

[25] T. Gao, P. S. Eldridge, T. C. H. Liew, S. I. Tsintzos, G. Stavrinidis, G. Deligeorgis, Z. Hatzopoulos, and P. G. Savvidis. Polariton condensate transistor switch. *Phys. Rev. B*, 85:235102, Jun 2012.

[26] Oleg L. Berman, Roman Ya. Kezerashvili, and German V. Kolmakov. Harnessing the polariton drag effect to design an electrically controlled optical switch. *ACS Nano*, 8(10):10437–10447, 2014. PMID: 25265156.

[27] Keliang He, Nardeep Kumar, Liang Zhao, Zefang Wang, Kin Fai Mak, Hui Zhao, and Jie Shan. Tightly bound excitons in monolayer wse_2. *Phys. Rev. Lett.*, 113:026803, Jul 2014.

[28] Xiaoze Liu, Tal Galfsky, Zheng Sun, Fengnian Xia, Erhchen Lin, Yi-Hsien Lee, Stéphane Kéna-Cohen, and Vinod Menon. Strong light-matter coupling in two-dimensional atomic crystals. *Nature Photonics*, 9, 06 2014.

[29] Frank Ceballos, Matthew Z. Bellus, Hsin-Ying Chiu, and Hui Zhao. Probing charge transfer excitons in a mose2–ws2 van der waals heterostructure. *Nanoscale*, 7:17523–17528, 2015.

[30] P. Cristofolini, G. Christmann, S. I. Tsintzos, G. Deligeorgis, G. Konstantinidis, Z. Hatzopoulos, P. G. Savvidis, and J. J. Baumberg. Coupling quantum tunneling with cavity photons. *Science*, 336(6082):704–707, 2012.

[31] T. Byrnes, G. V. Kolmakov, R. Ya. Kezerashvili, and Y. Yamamoto. Effective interaction and condensation of dipolaritons in coupled quantum wells. *Phys. Rev. B*, 90:125314, Sep 2014.

[32] Aubrey T. Hanbicki, Hsun-Jen Chuang, Matthew R. Rosenberger, C. Stephen Hellberg, Saujan V. Sivaram, Kathleen M. McCreary, Igor I. Mazin, and Berend T. Jonker. Double indirect interlayer exciton in a mose2/wse2 van der waals heterostructure. *ACS Nano*, 12(5):4719–4726, 2018.

[33] J.-J. Su and A. H. MacDonald. How to make a bilayer exciton condensate flow. *Nature Physics*, 4:799–802, 08 2008.

[34] O. L. Berman, R. Ya. Kezerashvili, and G. V. Kolmakov. Harnessing the polariton drag effect to design an electrically controlled optical switch. *ACS Nano*, 8(10):10437–10447, 2014.

[35] E. V. Calman, M. M. Fogler, L. V. Butov, S. Hu, A. Mishchenko, and A. K. Geim. Indirect excitons in van der Waals heterostructures at room temperature. *Nature Communications*, 9(1):1–5, May 2018.

[36] Wonbong Choi, Nitin Choudhary, Gang Hee Han, Juhong Park, Deji Akinwande, and Young Hee Lee. Recent development of two-dimensional transition metal dichalcogenides and their applications. *Materials Today*, 20(3):116 – 130, 2017.

[37] Y. N. Fernandez, M. I. Vasilevskiy, C. Trallero-Giner, and A. Kavokin. Condensed exciton polaritons in a two-dimensional trap: Elementary excitations and shaping by a gaussian pump beam. *Phys. Rev. B*, 87(19):195441, 2013.

[38] German V. Kolmakov, Leonid M. Pomirchi, and Roman Ya. Kezerashvili. Toward room-temperature superfluidity of exciton polaritons in an optical microcavity with an embedded mos2 monolayer. *J. Opt. Soc. Am. B*, 33(7):C72–C79, Jul 2016.

[39] B. Nelsen, G. Liu, M. Steger, D. W. Snoke, R. Balili, K. West, and L. Pfeiffer. Dissipationless flow and sharp threshold of a polariton condensate with long lifetime. *Phys. Rev. X*, 3:041015, Nov 2013.